Journal of Water Process Engineering 44 (2021) 102407

Contents lists available at ScienceDirect

Journal of Water Process Engineering

journal homepage: www.elsevier.com/locate/jwpe

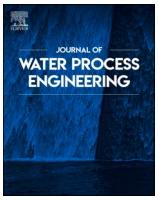

Recycled paper mill process water pre-treatment using ultrafiltration for water system closure

Hans Estrella Cainglet [a], Tomas Saavedra [b], Stefan Bürgmayr [c], Jianhua Zhang [d], Zongli Xie [e], Gil Garnier [c], Joanne Tanner [c,*]

[a] Department of Chemical and Biological Engineering, Monash University, Clayton, VIC 3800, Australia
[b] Department of Civil Engineering, Monash University, Clayton, VIC 3800, Australia
[c] Bioresource Processing Research Institute of Australia, Department of Chemical and Biological Engineering, Monash University, Clayton, VIC 3800, Australia
[d] Institute for Sustainable Industries and Liveable Cities, Victoria University, Werribee, VIC, 3030, Australia
[e] CSIRO Manufacturing, Clayton, VIC 3168, Australia

ARTICLE INFO

Keywords:
Ultrafiltration
Recycled paper mill
COD
Cake formation
Water system closure

ABSTRACT

The use of membranes in integrated water systems has garnered increasing attention in paper mills operating with virgin fibres, with documented closed water loops in industry. However, limited research exists on the performance of ultrafiltration (UF) in mills operating with 100% recycled fibres (RCF) and closed water systems, as these result in the introduction and accumulation of insoluble contaminants in the effluent. This study investigated the effect of transmembrane pressure (TMP) and feed organic load on the flux, types of fouling, and organic separation with UF membranes in a recycled paper mill using 100% RCF. The high feed organic load caused inevitable fouling, limiting the highest achievable flux. However, the TMP could be manipulated to improve on or exacerbate the process performance, within the range that was set as a result of the feed's characteristics. Low TMP (1.35 bar) generated the highest permeability and chemical oxygen demand removal, while higher TMPs produced higher fluxes and recoveries. The process was characterised by high initial fluxes, followed by cake formation, which dominated, and pore blockage. The excess cake formation induced cake filtration. This study shows the potential of UF membranes to be used as pre-treatment in filtering the process water in a recycled paper mill operating with 100% RCF, a critical step forward in implementing an integrated water system, and eventually closing the water loop.

1. Introduction

Papermaking requires large quantities of virgin fibres and water [1]. As a result, global trends such as the overexploitation and growing scarcity of natural resources continue to exert additional stress on the pulp and paper industry. In order to address this, two different approaches widely investigated include re-pulping of recycled fibres (RCF), and water system closure by recycling water streams [2]. The former has been reported to minimise waste generation and decrease pulping costs [3]. However, the introduction of RCF adds non-fibrous and insoluble contaminants, while system closure results in the accumulation of dissolved and colloidal materials, impeding the pulping process [4]. Consequently, there is a need to design efficient water treatment schemes to allow the streams to be fully reused for a sustainable closed loop water system (CLWS). One method gathering increasing attention is membrane filtration which was first investigated in the pulp and paper industry in the late 1960s [5]. Over time, membrane technology has proven to be a flexible and efficient treatment process for treating and reusing wastewater streams, due to the reduced variation in the quality of the effluents, and the simple automation of the processes [6].

Many studies have analysed the performance of membrane systems to treat water streams from virgin fibre production. Zhang et al. [7] investigated black liquor, pulp bleaching effluent, and paper machine white-water (PMWW) treatment in an integrated membrane process. This comprised physical and chemical pre-treatments, followed by a membrane bioreactor (MBR), microfiltration (MF), and reverse osmosis (RO). They noted that the MBR separated the majority of the soluble organic substances and suspended solids, ultimately achieving 60% recovery at the RO stage with acceptable permeate quality for mill reuse.

* Corresponding author at: Building 59, 15 Alliance Lane, Clayton, VIC 3800, Australia.
E-mail address: joanne.tanner@monash.edu (J. Tanner).

https://doi.org/10.1016/j.jwpe.2021.102407
Received 4 September 2021; Received in revised form 21 October 2021; Accepted 23 October 2021
Available online 4 November 2021

Richardson et al. [8] studied the feasibility of removing inorganic salts from PMWW to produce effluents acceptable for irrigation, using a multi-stage MF, ultrafiltration (UF), nanofiltration (NF), and RO pilot plant. However, they found that NF was unable to separate acceptable levels of sodium ions, resulting in excessive fouling at the RO stage. In addition, fouling was exacerbated by scaling in the RO membranes due to bicarbonate precipitation. The McKinley Mill in New Mexico has been operating with zero-effluent discharge since 1994 [9]. Their system comprises a disc-screen and cyclic activated sludge system as pre-treatment, followed by UF and RO, and an evaporative crystalliser. Their success lies in integrating their water treatment scheme into the paper mill's operational design. For instance, part of the UF membrane permeate is recycled into the mill's process water (PW), instead of the entire filtrate being sent to the RO membrane. The McKinley Mill demonstrates the importance of implementing the kidney approach in closing the water loop. This strategy focuses on directly treating and recycling internal effluents to reduce the operational strain of treating the end-of-pipe wastewater stream [10].

While success has been achieved for virgin fibre mills, there is limited research on the performance of membrane systems in mills using a fraction of recycled fibres. Negaresh [2] investigated NF as a pre-treatment to RO in a plant operating with 0 to 50% recycled newsprint fibre. They concluded that sodium and silica severely affected the performance of the membrane, achieving only 22% water recovery at the RO stage at 50% RCF. Richardson et al. [11] treated 40% RCF filtrate using a three-stage UF, NF, and RO pilot plant, noting that fouling at the NF stage prevented the implementation of such system. Eventually, the pilot plant was decomissioned as excessive fouling could not be controlled due to the lack of process optimisation. Particularly, they were unable to reduce the chemical oxygen demand (COD) to acceptable levels prior to the NF stage, which could have potentially been achieved with sufficient pre-treatment, as observed in the McKinley Mill.

So far, there have been no published investigations on the performance of UF in mills operating with 100% RCF and restricted water systems, as the majority of industrial UF membranes employed in the pulp and paper industry are used to recover coating colours and to treat PMWW [5]. Since UF is the most widely used and established membrane process in the pulp and paper industry, and therefore has considerable existing infrastructure and associated operational knowledge, it seems sensible to explore its potential for broader applications, including CLWSs in recycled paper mills. One of the major hindrances to the implementation of membrane technology in any industry is membrane fouling [5], a challenge also identified for membrane filtration of RCF [11], as the permeate flow is inherently governed by fouling [12]. Four fouling mechanism models for ultrafiltration membranes were developed by Hermia [13]: complete blocking, intermediate blocking, standard blocking, and cake layer formation. The causes for the fouling phenomena can be inferred by analysing the effects of transmembrane pressure (TMP) and feed organic load on the fouling type and flux. Little research exists on the applications of these models in mills using RCF. Sousa et al. [14] applied them, however, their feed was sourced from the wastewater treatment plant of the recycled paper mill, reducing the concentration of contaminants. They concluded that the mechanism controlling fouling was intermediate blocking. Xu et al. [15] investigated fouling mechanisms in a recycled paper mill, however their focus was on the performance of using upstream coagulation and Fenton pre-treatment prior to UF.

Ultimately, with the success of closed loops in mills operating with virgin fibres, there is high potential to achieve system closure in recycled paper mills when using the kidney approach. In addition, there is a lack of knowledge on the fouling modes for ultrafiltration membranes in such mills, as well as the PW characteristics. This inhibits the development of sustainable effluent management and water closure systems, as observed in the decommissioned pilot plant by [11]. UF systems are pressure-driven processes, and RCF effluents are characterised by high COD, which may vary drastically from day to day due to the heterogeneous nature of the recycled feed. This study therefore investigated the effects of TMP and organic load on the fouling mechanisms in UF membranes when treating the PW from a recycled paper mill operating with 100% RCF. The resulting flux and quality of the permeate were also investigated. As a result, a critical foundation was determined for the potential use of ultrafiltration membrane technology as pre-treatment using the kidney approach. By evaluating UF's performance in filtering the process water in mills fully operating with RCF, this study provides a critical step forward in integrating a complete water treatment scheme, and eventually closing the loop towards cleaner production.

2. Materials and methods

2.1. Recycled paper mill process water

The feed was taken from a clarifier with a 20-micron disc filter from the Visy Coolaroo mill – experimental section, in Australia. When investigating the organic load's effect on the rate and type of fouling, 100% and 50% PW solutions (by volume) were used. The solvent employed was tap water (TW) for 50% dilutions, as the presence of ions would not have affected the UF membrane performance due to the filter's pore sizes [16]. When not in use, the feed was stored in a 4 °C fridge. Spectrum™ RX9100 microbiocide agent was added five days after collecting the feed to prevent the degradation of the organic matter [17]. The microbiocide agent, composed of bronopol, methylchloroisothiazolinone, and methylisothiazolinone, was sourced from Solenis.

2.2. Process water and membrane characterisation

COD and non-purgeable dissolved organic carbon (NPOC) of the process water, both diluted and undiluted, were measured using Spectroquant® Prove 300 Spectrophotometer and Shimadzu TOC-V with TNM-1unit respectively. The error bars shown in Fig. 10 are based on the error measurements of the equipment. The spectrophotometric methods were adapted from the Standard Methods for the Examination of Water and Wastewater [17]. pH, electrical conductivity (EC), and temperature were measured using Thermoscientific Orion Star™ A325 pH/Conductivity Portable Multiparameter meter. The size distribution of the particles in the water samples were measured using laser diffraction in a Malvern Mastersizer 2000. The target analyte was $CaCO_3$ (calcite), with obscuration averaging 6.87%. Deionised (DI) water was used as dispersant.

Scanning electron microscope (SEM) images of the membrane surfaces were captured using Phenom XL Benchtop SEM for qualitative fouling analysis. The images were analysed at 1000× and 2500× magnification using full backscatter electron detector and 15 kV. The beam intensity was set to image with 1024 resolution. Energy Dispersive X-Ray (EDX) analyses were conducted using the built-in software to identify the elements present on the membrane surfaces. Prior to the SEM analysis, the membrane samples were sputter coated with gold/platinum for 15 s using Quorum SC7620 Sputter Coater.

2.3. Experimental setup

The membranes used were polyethersulphone Synder® UF flat-sheet membranes (MQ model); 50 kDa MWCO with 42 cm^2 active surface area. The membrane module was a Sterlitech CF042H. The experiments were conducted using the setup shown in Fig. 1, where PG corresponds to a manometer showing the gauge pressure. Each trial ran for 1.5 h. Prior to each run, the membranes were preconditioned with DI water for 30 min to establish the pure water flux baseline and remove any impurities from the membranes. Constant pressure mode and crossflow regime were used. A new membrane was used for each experiment.

The feed was stored in a graduated cylinder and pumped over the membrane using a Hydra-Cell G13 centrifugal pump. The transmembrane pressure was set by manually adjusting the opening pressure

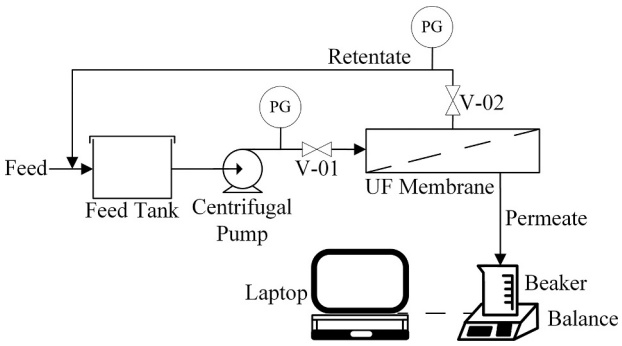

Fig. 1. Experimental setup flowsheet.

of check valve V-02. The permeate was collected in a beaker placed on top of a balance, which recorded the permeate mass every 60 s. At the end of each experiment, 40 mL permeate samples were collected for COD and NPOC measurements. The membranes were dried at room temperature and then stored in press seal plastic bags to be analysed by SEM. The retentate was continuously recycled to minimise the initial feed volume required. The initial feed volume was maintained at 1.6 L. The crossflow velocity averaged 1.50 m/s.

2.4. Flux analysis

The permeate flow rate was calculated by dividing the difference of consecutive weight measurements by the timestep and multiplying the results with the density of water, assumed constant at 20 °C (0.998 g/mL). The fluxes were calculated by dividing the permeate flow rate by the active surface area of the membrane. These were then adjusted by standard temperature (20 °C) based on [18], as shown in Eq. (1). [12]. The flux reductions in percent over time were calculated using Eq. (2). The recovery for each experiment was calculated using Eq. (3).

$$J_s = J_m \frac{\mu_m}{\mu_s} = J_m (1.03)^{T_s - T_m} \tag{1}$$

$$J_{s\ (reduction\%)} = \frac{J_{s(i)} - J_{s(i+1)}}{J_{s(i)}} \times 100 \tag{2}$$

$$Recovery\ (\%) = \frac{Permeate\ volume\ at\ the\ end\ of\ each\ experiment}{Starting\ feed\ volume} \times 100 \tag{3}$$

where $_s$ and $_m$ correspond to standard and measured values, J is the permeate flux (L/m^2·h), T is temperature, and μ is the dynamic viscosity of the feed, with μ_m assumed to be the same as water at 20^o C (1.00 × 10^3 kg/m·s). (i) corresponds to the flux recorded at time i. The specific flux normalised the temperature-adjusted flux by TMP. This can be found in Eq. (4). The error bars shown in Fig. 6 are based on the standard deviation of the last five flux measurements for each experiment. The resulting specific fluxes of each experiment were also normalised by the permeability of DI water to compare the specific fluxes across different TMPs. This is because the permeability can be affected by membrane compaction, fouling layer compaction, and general resistance with increasing feed pressure. This is shown in Eq. (5). The specific flux results were also used to determine the performance loss due to fouling, depicted in Eq. (6) [12].

$$J_{sp} = \frac{J_s}{\Delta P} \tag{4}$$

$$J_{sp\_norm} = \frac{J_{sp-PW}}{J_{sp-DI\ water\ at\ the\ same\ TMP}} \tag{5}$$

$$Performance\ drop\ due\ to\ fouling\ (\%) = \frac{J_{sp(a)} - J_{sp(b)}}{J_{sp(a)}} \times 100\% \tag{6}$$

where J_{sp} is the specific flux at standard temperature (L/m^{2}h·bar). (a) and (b) correspond to the point of reference and flux that is being evaluated.

3. Model description

Modelling the fouling mechanisms is essential to evaluate the causes of fouling, which is key in determining the ability of membrane technology to treat the process waters in paper mills fully operating with recycled fibres. Understanding the fouling phenomena is also critical to understanding the effect of TMP and feed organic load on the filtration process. A limitation of the Hermia model is that it was developed for dead-end filtration mode, whereas most industrial processes, as well as the experiments conducted here, use crossflow configuration. de Barros et al. [19] modified Hermia's model to account for this. The general form for the adjusted models can be found in Eq. (7). All these models assume that the membrane is composed of parallel pores with constant diameters and heights [13].

$$-\frac{dJ}{dt} = k(J - J_{ss})^{2-n} \tag{7}$$

where t is the filtration time. k corresponds to the blocking law filtration coefficient. The equation to calculate k differs for all four models and details are available in [19]. n corresponds to the fouling mechanism: 2.0 for complete blocking, 1.5 for standard blocking, 1.0 for intermediate blocking, and 0 for cake filtration. The fouling mechanisms modified by [19] are illustrated in Fig. 2.

3.1. Complete blocking model ($n = 2$)

The complete blocking model assumes the entrance of the pores gets blocked due to particle retention [13]. Also, it posits that the particles land only on the membrane, not on each other. The flux decline is proportional to the covered area and reaches zero when a monolayer is formed [19]. The corresponding flux equation can be found in Eq. (8), and is depicted in Fig. 2a.

$$J_m = J_{ss} + (J_0 - J_{ss}) * e^{-k_c * t} \tag{8}$$

3.2. Standard blocking model ($n = 1.5$)

The standard blocking model accounts for the reduction of the void volume within the membrane. It assumes the pore volume decreases proportionally to the volume of particles that are uniformly deposited on the pore walls [13]. The corresponding flux equation can be found in Eq. (9), and is represented in Fig. 2b.

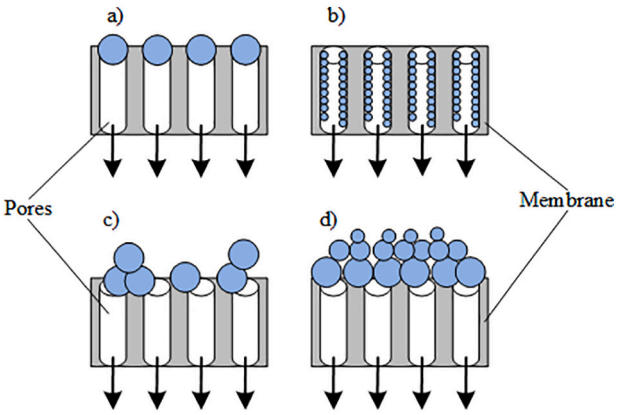

Fig. 2. Fouling mechanisms: a) complete blocking model; b) standard blocking model; c) intermediate blocking model; d) cake filtration model. Adapted from [19].

$$J_p = \frac{1}{\left(\sqrt{\frac{1}{J_0}} + k_s * t\right)^2} \quad (9)$$

3.3. Intermediate blocking model ($n = 1$)

The intermediate blocking model is an extension of the complete blocking model. It still assumes that the pore entrances are blocked, but allows for particles to land on top of one another, and for blocked pores to be subsequently unblocked [13]. Consequently, the probability of a particle blocking a pore is modelled. The corresponding flux equation can be found in Eq. (10), and is shown in Fig. 2c.

$$J_m = \frac{J_0 * J_{ss} * e^{-k_i * J_{ss} * t}}{J_{ss} + J_0 * (e^{-k_i * J_{ss} * t} - 1)} \quad (10)$$

3.4. Cake filtration model ($n = 0$)

Based on resistance-in-series, the cake filtration model assumes that the retained particles do not affect the membrane structure [20]. In other words, pore blocking and constriction do not take place. Instead, cake formation occurs on the membrane outer surface due to large particles. The corresponding flux equation can be found in Eq. (11), and is depicted in Fig. 2d.

$$J_{ss}^{\ 2} * k_0 * t = ln\left(\frac{J_p * (J_0 - J_{ss})}{J_0 \quad J_m - J_{ss}}\right) - J_{ss} * \left(\frac{1}{J_m} - \frac{1}{J_0}\right) \quad (11)$$

4. Results and discussion

4.1. Feed characteristics

UF membranes are known to remove organic matter and particles, although fouling is often caused by these particles, and other organic and biological contaminants [12]. Cake formation occurs due to large particles, while pore blockages and pore volume reductions result from the smaller ones. This study evaluated the reduction of COD with UF. Non-purgeable organic carbon (NPOC) was measured to corroborate the COD results. COD is influenced by the high amounts of total suspended solids such as fibres, and oxidisable wet-end additives such as starch, in the process water [10]. The feed characteristics for 100% and 50% PW are shown in Table 1. The COD and NPOC values for 100% PW were taken over four non-consecutive days. The COD and NPOC of a 50% PW feed sample were measured and compared with the 100% PW feed sample that was taken on the same day (third) of sampling. Because the 50% PW feed COD and NPOC both averaged 53% of the original 100% PW, and the COD and NPOC measurements were within the error measurements of the analytical method, the characteristics of the single sample was taken as representative for all 50% PW feeds.

The initial feed temperatures varied depending on the ambient conditions. However, the temperatures increased throughout all experiments due to increase in ambient room temperature. The final feed temperatures at the end of the 100% and 50% PW runs averaged 22.90 °C ± 1.28 °C and 23.90 ± 0.61 °C, respectively. The average particle size distribution (PSD) for 100% PW is shown in Fig. 3. A bimodal distribution is observed with two major peaks at 1 and 100 μm.

Table 1
Feed properties for 100% and 50% process water (PW) ($*n = 4$, $\hat{}n = 1$, $^{>}n = 6$, $^{<}n = 3$).

Characteristics	100% PW	50% PW
COD (mg/L)	8227 ± 200*	4145$^{\hat{}}$
NPOC (mg/L)	2368 ± 46*	1170$^{\hat{}}$
pH	5.73 ± 0.027$^{>}$	5.92 ± 0.012$^{<}$
EC (mS/cm)	3.96 ± 0.060$^{>}$	2.24 ± 0.021$^{<}$
Temperature (°C)	13.59 ± 1.62$^{>}$	18.27 ± 0.63$^{<}$

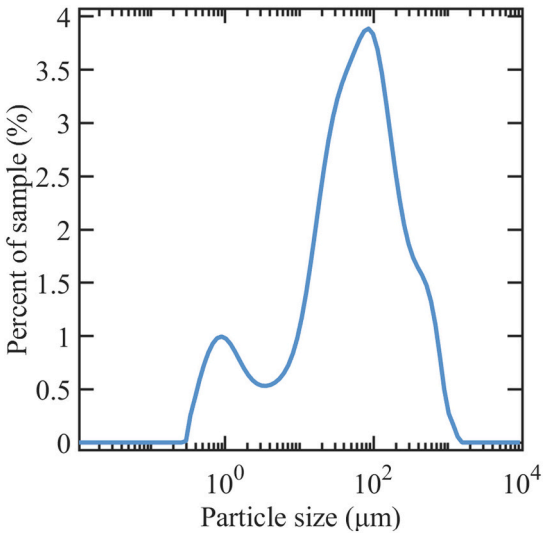

Fig. 3. Average particle size distribution of process water (100%) ($n = 4$, σ = 0.085).

Two other peaks are observed at around 50 and 400 μm, but were excluded due to their low impact and significance compared to the local peaks. The high concentration of larger particles suggests that fouling can easily occur.

4.2. Flux

To determine the effect of organic load and TMP on flux, experiments were conducted at 50% and 100% PW for TMPs of 1.35, 4.5, and 6 bar for 1.5 h. The flux data were adjusted by temperature to account for the varying viscosity of the feed due to temperature changes, as temperature was not controlled. The resulting fluxes for 50% and 100% PW at all TMPs are shown in Fig. 4. The flux reductions in percent were calculated to further evaluate the process behaviour, as seen in Fig. 5.

Low TMP (1.35 bar) resulted in lower fluxes. 50% PW at 1.35 bar TMP had an initial flux of 46 L/m^2·h which was reduced to 32 L/m^2·h within the second minute, and continued to decrease throughout the experiment. The flux for 100% PW at the same TMP did not decrease as drastically within the first 2 min of the run, and also steadily decreased throughout the experiment. The 1.35 bar TMP fluxes were reduced by 42% after 90 min, whereas at higher TMP, flux reductions averaged over 59%.

Although the 50% PW fluxes seem to be declining more severely compared to 100% PW towards the end of each experiment, and higher TMP produced higher volumetric flux reductions, Fig. 5 shows that all combinations of TMP and PW experienced similar percent flux reductions, ranging between −5% and 10% after the first 10 min. Notwithstanding, the steeper volumetric flux drops observed with increasing TMP are attributed to the large driving force across the membrane, which may have exacerbated fouling. Sousa et al. [14] and Xu et al. [15] reported similar initial flux reductions at TMPs above 1 bar. With feed COD levels at 252 and 733 mg/L respectively, they seemingly had consistent percent flux reductions, likewise to the data shown in Fig. 5.

Fig. 5 suggests that the feed organic load limited the allowable flux, contributing more severely to fouling. However, Fig. 4 shows that TMP can be manipulated to produce higher permeate flow rates, and therefore, can be modified to exacerbate or limit the effects of fouling. This is seen in the difference in flux reductions during the first 10 min between low and high TMP in Fig. 4, implying that significant and immediate fouling is mainly observed at TMPs above 1.35 bar.

The permeate recoveries are summarised in Table 2. The recoveries for both feed concentrations increased from 1.35 bar to 4.5 bar TMP,

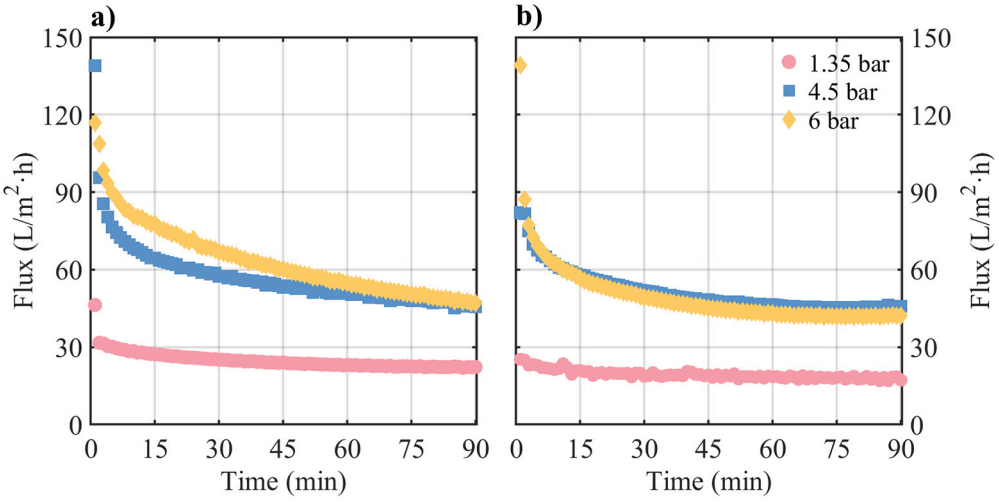

Fig. 4. Permeate flux decline over time at various TMP for: a) 50% PW; b) 100% PW.

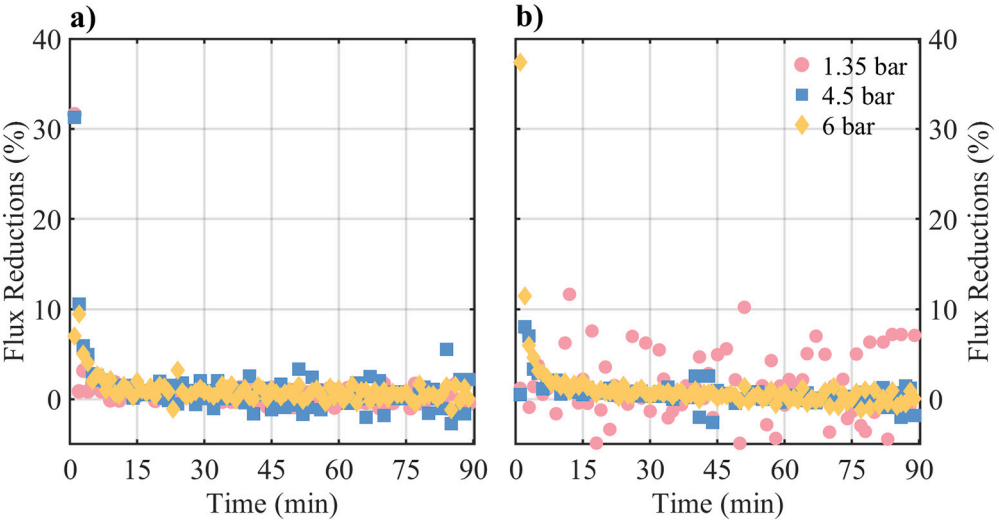

Fig. 5. Permeate flux reductions in percent over time at various TMP for: a) 50% PW; b) 100% PW.

Table 2
Permeate recoveries for 100% and 50% PW across all TMP.

TMP (bar)	100% PW recovery (%)	50% PW recovery (%)
1.35	8%	11%
4.5	21%	25%
6	21%	29%

after which the recoveries achieved were similar from 4.5 to 6 bar TMP. The recoveries for 50% PW were consistently higher compared to 100% PW, with the differences attributed to 50% PW not having as drastic initial flux reductions. As seen in Fig. 4, 50% PW 6 bar TMP did not drop as severely as 4.5 bar TMP with the same concentration within the first 30 min, justifying its higher recovery.

The low recoveries are due to the duration of the experiments. A single run with 100% PW at 4.5 bar TMP was conducted for 2.5 h. Although the feed volume was increased from 1.6 to 2 L, the permeate recovery reached 32%. Further studies are required to investigate the process behaviours at longer operating times.

4.3. Specific flux and performance loss due to fouling

To compare the process performances across different TMPs and feed concentrations, the specific and normalised specific fluxes, based on the fluxes recorded at the 90-minute mark, were calculated. Because the specific flux, also known as permeability, indicates the permeate flow rate per area per unit of pressure applied, it can be used to infer the process energy requirements. The permeabilities for 50% and 100% PW at all TMPs are shown in Fig. 6. Normalising the specific fluxes for both feed concentrations with DI water generates the percent of permeability achieved at each TMP, as shown in Table 3.

The specific flux for DI water increased from 1.35 to 4.5 bar, and decreased again after. This is attributed to higher membrane resistance because of compaction, which was caused by the high feed pressure. In other words, despite 6 bar TMP producing higher permeate flow rates (see Fig. S1 in the Supplementary information), the increase in flux from 4.5 to 6 bar TMP was not high enough to match the efficiency of operating at 4.5 bar. However, when using 100% and 50% PW, both the permeability and normalised specific flux decreased as TMP increased, with both feed concentrations reaching similar values at 4.5 and 6 bar TMP.

50% PW 1.35 bar TMP produced the largest specific flux,

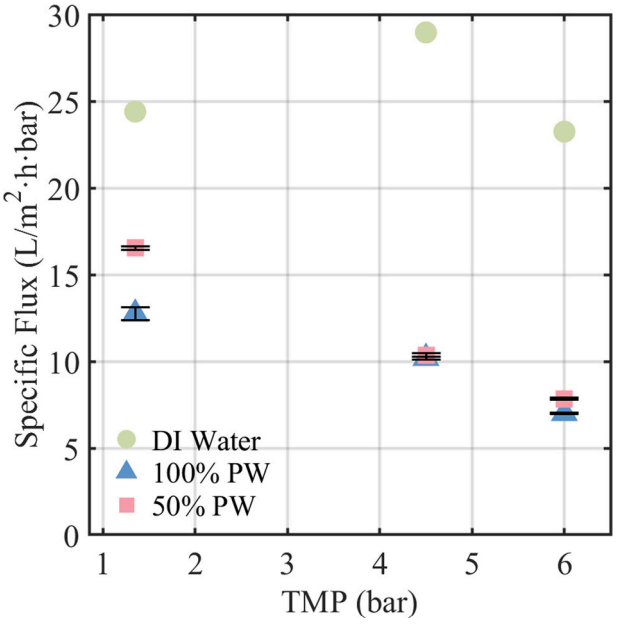

Fig. 6. Specific fluxes at various TMP for DI water, 50% PW, and 100% PW.

Table 3
Specific flux normalised by DI water at each TMP.

TMP (bar)	100% PW (%)	50% PW (%)
1.35	52%	68%
4.5	35%	36%
6	30%	34%

significantly higher compared to 100% PW at the same TMP, as seen in Table 3. This suggests that 50% PW 1.35 bar was the most efficient separation process, due to the low feed pressure and reduced number of particles, reducing the negative effects of fouling. Notwithstanding, 1.35 bar had a significantly higher normalised specific fluxes compared to higher TMPs for both feed concentrations. It can be seen that 1.35 bar TMP and 50% PW produced the highest permeabilities and normalised specific fluxes, both representing the most efficient separation conditions for this process. Therefore, 100% and 50% PW at 1.35 bar TMP were used as reference points to evaluate the performance drop when operating at higher TMPs for 100% and 50% PW respectively, as shown in Table 4. Table 5 presents the performance drop when operating with 100% PW feed, using 50% PW feed as baseline. The values in both tables are the averages throughout the experiments.

A significant increase in performance loss at higher TMP is noted in Table 4, demonstrating the exacerbating effects of TMP on fouling, and its resulting effect on performance. Because 50% PW 1.35 bar TMP was more efficient compared to 100% PW 1.35 bar TMP, the performance drop was more severe when operating at higher TMP for 50% PW.

Table 5 indicates that 100% PW 4.5 bar TMP was a relatively efficient process condition. The performance drop when increasing the TMP from 1.35 bar to 4.5 bar at 100% PW was only 20%. Furthermore, the drop in performance when operating at 100% PW versus 50% PW for 4.5 bar TMP was only 3%.

Table 4
Performance loss in percentage relative to the baseline performance at 1.35 bar TMP due to increased fouling at higher TMP.

TMP (bar)	100% PW	50% PW
4.5	20%	39%
6	45%	52%

Table 5
Performance loss in percentage relative to the baseline performance of 50% PW feed due to increased fouling at higher organic load.

1.35 bar TMP	4.5 bar TMP	6 bar TMP
20%	3%	12%

Except for 1.35 bar TMP, the performance drops listed in Table 5 are considerably lower compared to Table 4. These results, in addition to those presented in Fig. 6. and Table 3, show that both the TMP and feed organic load affected fouling. Likewise to the findings detailed in Section 4.2, the feed COD limited the highest achievable process performance. However, TMP controlled the extent of fouling within the range specified by the feed organic load. Consequently, TMP can be construed as the dominant factor that controls fouling, as it can be manipulated to improve on or exacerbate the process performance, given that fouling is inevitable due to the high number of particles in the feed.

Reducing the feed COD from 8200 to 4100 mg/L did not have as significant an impact on the process performance as changing the TMP. The reduced influence of the feed organic load on the extent of fouling can be explained by 1.35 bar achieving comparable recoveries (Table 2) for both feed concentrations, despite 50% PW leading to more efficient process conditions. This is also supported by the significantly similar permeabilities and normalised specific fluxes achieved with both feed concentrations at 4.5 and 6 bar TMP. These results have important implications for industrial processes as they indicate that there are trade-offs between obtaining high permeate flow rates (achieved at higher TMP) while simultaneously minimising energy consumption and fouling (achieved at lower TMP).

4.4. Fouling

4.4.1. Model results

To identify the fouling mechanisms, the four adjusted fouling mechanisms developed by Hermia [13] and summarised in Section 3 were fitted to the flux data for 100% and 50% PW. Table 6 presents the coefficient of determination (R^2) values obtained for each blocking model. An example of this fit for 100% PW at 6 bar TMP is shown in Fig. 7. Cake formation was the dominant mechanism for all combinations of feed and TMP, despite 100% PW at 4.5 bar TMP recording a slightly higher fit for intermediate blocking.

Standard blocking and complete blocking are simplistic models, as the pore volume distribution of the membranes is assumed to be uniform. Because the standard blocking model accounts for particle impingement and gradual pore volume reduction, its predicted flux steadily decreases without plateauing, as seen in Fig. 7b. The complete blocking model is restrictive because of its monolayer assumption,

Table 6
Summary of R^2 values reached by each combination of feed and TMP. The bold R^2 values correspond to the dominant fouling mechanism(s) for each combination of feed and TMP.

Feed	TMP (bar)	R^2			
		Complete blocking	Standard blocking	Intermediate blocking	Cake formation
100% PW	1.35	0.74	−0.01	0.79	**0.82**
100% PW	4.5	**0.97**	0.17	**0.98**	**0.97**
100% PW	6	0.77	−1.53	0.88	**0.92**
50% PW	1.35	0.60	−2.64	0.72	**0.77**
50% PW	4.5	0.60	−1.42	0.78	**0.90**
50% PW	6	0.90	0.59	**0.96**	**0.97**

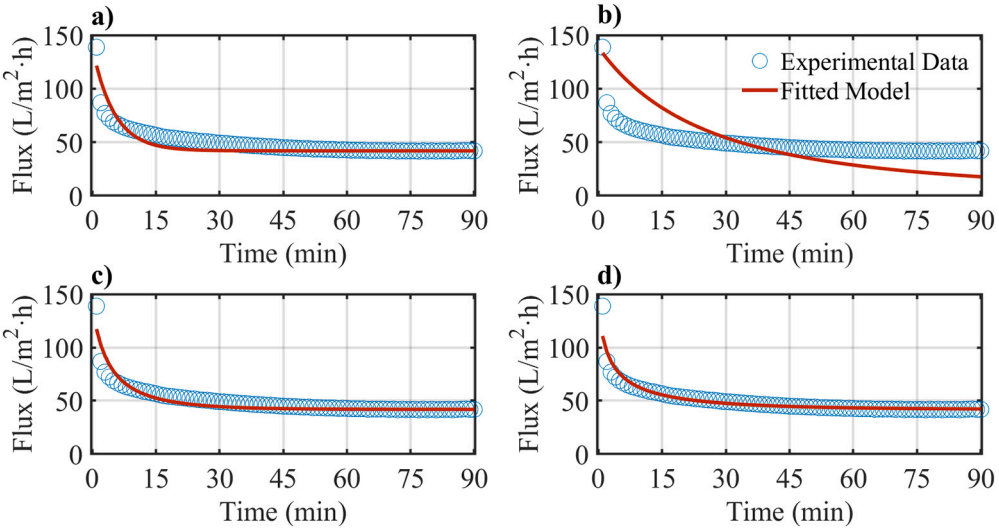

Fig. 7. 100% PW 6 bar TMP plotted over each fitted model for a) complete blocking model ($R^2 = 0.77$); b) standard blocking model ($R^2 = -1.53$); c) intermediate blocking model ($R^2 = 0.88$); d) cake formation model ($R^2 = 0.92$).

justifying the consistently better fit of the intermediate blocking model to the experimental results, regardless of feed concentration and TMP. As seen in Fig. 7a, the flux predicted by the complete blocking model theoretically reaches steady-state immediately, while that predicted by the intermediate blocking model (Fig. 7c) allows for continuous small reductions after the initial flux drop. The complete and standard blocking model predictions do not adequately match the experimental results shown in Fig. 4, wherein all fluxes were continuously reduced over time, with fluxes above 1.35 bar TMP experiencing severe initial drops.

50% PW at 1.35 bar TMP had lower fits for all models compared to the other process parameters. This is attributed to its high normalised specific flux (Table 3), indicating reduced fouling. The lower normalised specific flux for 100% PW 1.35 bar indicates that more severe cake formation occurred compared to 50% PW at the same TMP, supported by the higher R^2 fit in Table 6. This was attributed to the higher feed contaminant levels.

100% PW 4.5 bar TMP had high fits for the complete blocking, intermediate blocking, and cake formation models. The high complete blocking model fit indicates that pore blockage indeed occurred for 100% PW 4.5 bar TMP, but that the feed pressure was not high enough to increase the force with which the particles collided with the membrane surface, achieving more stable flow. This further supports the results presented in Section 4.3, where 100% PW at 4.5 bar was shown to be an efficient combination of feed and process conditions. Notwithstanding, cake formation appears to dominate, as will be discussed in Section 4.4.2.

Sousa et al. [14] applied the Hermia [13] cake filtration model when treating the wastewater from a recycled paper mill. At TMPs equal to and above 2 bar, their dominant fouling mechanism was intermediate blocking due to their significantly smaller feed PSD (0.1589–1.642 μm) and COD levels (252 mg/L). The standard blocking model had a low fit to their data, implying that the model poorly predicts the fouling behaviour for feeds with multiple contaminants and non-uniform PSD. The results of [14] agree with our findings. Their smaller PSD contributed more to pore blockage, whereas the larger and bimodal PSD of our process water (Fig. 3) appears to result in a combination of pore blockage (smaller particles) and cake formation (larger particles), with the latter occurring more intensely due to the higher number of larger particles.

Consequently, the feed PSD and organic load dictate the type and extent of each fouling mechanism, while the severity of fouling is attributed more highly to TMP. It is worth noting that in this study, the 50% PW already contained high organic concentrations (4000 mg/L COD). Therefore, all membranes experienced cake formation, although 50% PW was less intense. The feed organic load would have to be as low as those explored by [14] to reduce the occurrence of cake formation. Our conclusion is supported by the fact that [14] did not get adequate fits for any model at TMPs below 2 bar, as the low pressure did not induce fouling as severely as higher TMPs. Likewise, in this study, 1.35 bar TMP had lower (R^2) fits for all models for 50% and 100% PW.

These conclusions corroborate the findings detailed in Section 4.3. In our process, the feed organic load limited the achievable specific flux due the high number of particles, both small and large, contributing to pore blockage and cake formation. However, the TMP dictated the severity and extent of the fouling mechanisms, controlling the process performance. Ultimately, the process can be characterised by a mixture of layered pore blockages and dominant cake formation for all combinations of feed organic load and TMP.

4.4.2. Morphology

SEM images of the UF membranes following use with DI water and PW at different feed concentrations and TMP are shown in Fig. 8. DI water (Fig. 8a) was used as reference to enable the degree of fouling for the other membranes to be visually evaluated. The pores of the membrane exposed to DI water were clear and numerous, and the membrane surface was smooth. The SEM images for 100% PW 1.35 and 4.5 bar TMP at higher magnification are shown in Fig. 9 to further visualise the increased occurrence of fouling at higher TMP.

The surface of the membrane exposed to 100% PW at 1.35 bar is significantly less smooth compared to the membrane operated solely with DI water. However, the number of unblocked pores remains quite high in Fig. 8b, suggesting that fouling was not as severe as the membranes operated at higher TMPs (Fig. 8c–f). The rough surface is attributed to cake formation. EDX indicated the presence of sodium and calcium on the PW-based membrane surfaces, while the DI water membrane surfaces had none (see Figs. S2 and S3).

100% PW at 4.5 bar TMP (Fig. 8c) appears to be slightly more fouled compared to 50% PW at the same TMP (Fig. 8d), due to its surface being less smooth, with increased calcium-rich blocked pores (bright circles), as seen in Figs. 8c and S4. This is justified as 50% PW 4.5 bar was only slightly more efficient compared to 100% PW at the same TMP (Table 5). The fewer blocked pores and areas with smoother surface in Fig. 8d indicates reduced cake formation. These observations support the R^2 data shown in Table 6. Nevertheless, the difference in fouling phenomena and intensity from 1.35 to 4.5 bar TMP 100% PW is clear from

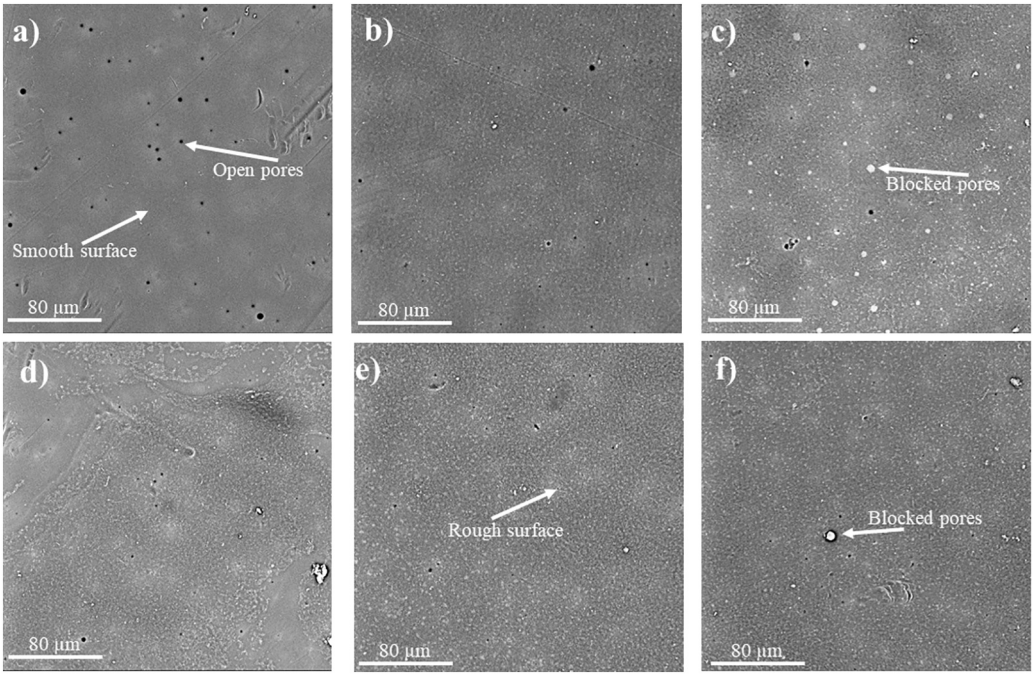

Fig. 8. SEM images of membranes; a) DI water; b) 100% PW 1.35 bar TMP; c) 100% PW 4.5 bar TMP; d) 50% PW 4.5 bar TMP; e) 100% PW 6 bar TMP; f) 50% PW 6 bar TMP.

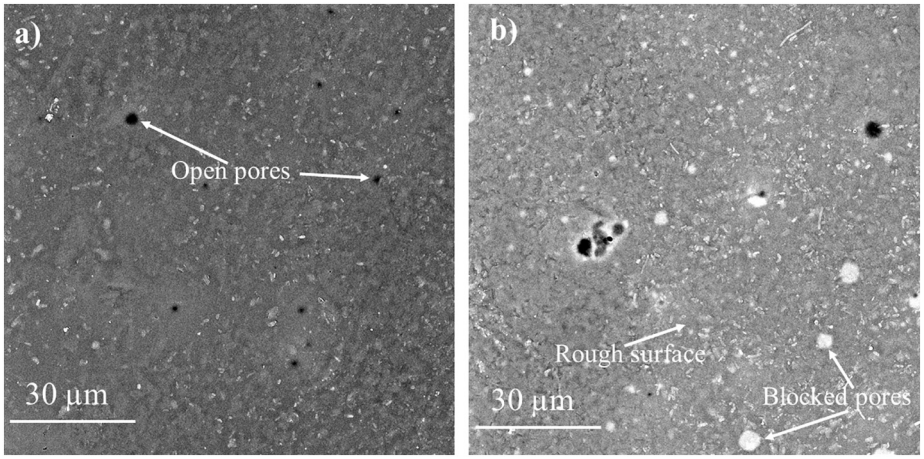

Fig. 9. SEM images at higher magnification membranes; a) 100% PW 1.35 bar TMP; b) 100% PW 4.5 TMP.

Fig. 9, with a rougher surface and blocked pores observed in Fig. 9b.

100% and 50% PW at 6 bar TMP (Fig. 8e and f) show clear signs of cake formation with moderate pore blockages. This explains why both feed concentrations at 6 bar TMP are good fits for the Hermia intermediate blocking and cake formation models, as increased cake formation at higher contaminant concentrations and TMP increased the probability of pore blockage, which is modelled by intermediate blocking. The similarity in the visual extent of fouling supports the findings detailed in Section 4.3 that the high feed pressure of 6 bar forced the particles onto the membrane, exacerbating fouling, which was not as severe for 4.5 bar TMP for both feed concentrations.

Xu et al. [15] investigated the effect of coagulation and Fenton pretreatment on the performance of UF in treating the secondary effluent from a recycled paper mill. They did not fit their flux data to the Hermia [13] model. However, with feed COD loads amounting to 733 mg/L, the SEM images of their membrane surfaces were relatively smooth, with only moderate signs of pore blockage and cake formation. This supports the hypothesis that the fouling type is more heavily influenced by the feed PSD. In addition, SEM analysis corroborates the findings that pore blockage and cake formation occurred regardless of the PW and TMP used. Visually comparing the membranes supports the hypothesis that TMP controls the severity with which fouling occurred, and its resulting effect on the process performance. These also support our previous findings of increased fouling with increasing TMP.

Ultrafiltration in flat-sheet membranes is traditionally characterised by high initial fluxes, followed by immediate and drastic fouling, after which steady-state flow rapidly occurs, as demonstrated by [21]. In this study, high initial fluxes were achieved within the first minute of each experiment. These were followed by drastic flux reductions during the succeeding 9 min (Figs. 4 and 5), attributed to pore blockage and cake formation. Then, cake filtration was achieved, characterised by the consistent low percent flux reductions. The divergence is attributed to the difference in feed characteristics, as [21] used dilute suspensions of polystyrene particles compared to this study's highly concentrated PW,

characterised by high COD levels, large particles, and a large PSD.

4.5. Separation performance

To determine the effect of organic load and TMP on organic separation, the COD and NPOC of the permeates were analysed for 50% and 100% PW at all TMPs, and compared with their original feed organic loads. Fig. 10a and b shows the COD and NPOC concentrations for 50% and 100% PW permeates at different TMPs. Fig. 9c and d highlights the percent reductions of COD and NPOC in the permeate from their original feed concentrations. The same trends are observed for both COD and NPOC permeate measurements. Although a pattern is observed for the 50% PW permeate organic loads, the values are within the experimental error. Therefore, it can be concluded that at 50% PW concentration, the percent organic load reduction is almost identical across all TMPs. Conversely, for 100% PW permeates, the organic load increased with from 1.35 to 4.5 bar, and decreased again as TMP increased further.

The differing organic removal trends are due to the increased cake formation at 100% PW, attributed to the higher number of particles in the feed. This explains the increased COD removal at 6 bar TMP for 100% PW, as the higher feed pressure forced the water through the cake, simultaneously causing more severe cake formation while rejecting COD, as discussed in Section 4.4.2 (Fig. 8e and f). On the other hand, low TMP (1.35 bar) produced high organic removal for 100% PW, attributed to the lower pressure which reduced the severity with which particles interfered with each other on the membrane surface, resulting in more efficient organic separation. The uniform organic removal for 50% PW (Fig. 9c) is attributed to the reduced particle interference on the membrane surfaces, reducing the resistance with which water was filtered through the membrane. This indicates that at half the organic load, both the specific flux (Fig. 6) and contaminant reduction are similar at high TMP (4.5 to 6 bar).

Sousa et al. (2018) [14] and Xu et al. (2018) [15] both investigated the COD separation in their processes. Although their membrane MWCOs were 10 and 5 kDa, their COD removal amounted to 54% and 48%, respectively. Conversely, the highest COD separation achieved in the current study was 47%. This suggests that high quality separation can be achieved if UF is operated in series, as despite the large disparity in feed organic concentration, the removal efficiency is high. Filtration can be further improved if backwashing is implemented, as cake formation is reversible. These are key factors that need to be investigated in future studies, as their influence on the process conditions and separation capabilities are critical in implementing a water treatment scheme to close the water system loop in paper mills operating with recycled fibres.

5. Conclusion

Despite the success of closed loops in paper mills operating with virgin fibres, limited information exists on the performance of UF in mills operating with 100% RCF and restricted water systems, as these result in the accumulation of insoluble contaminants in the effluent, straining the water treatment process. This study investigated the effects of transmembrane pressure and organic load on the flux, types of fouling, and organic separation capabilities in a recycled paper mill using 100% RCF. The flux reductions consistently ranged from −5% to 10% after the first 10 min of each experiment. The performance drop when operating at higher TMP reached 52% (6 bar TMP 50% PW), whereas doubling the feed COD from 4100 mg/L to 8200 mg/L only reached up to 20% drop in performance (1.35 bar TMP 100% PW).

For 100% PW, low TMP (1.35 bar) produced the highest specific flux (13 L/m^2·h·bar) and COD reduction (47%), whereas higher TMP produced higher permeate flow rates, with 4.5 bar TMP generating a moderately efficient process. While 4.5 to 6 bar seemed to optimise the flux and recovery for this process, low TMP appears to be the more sensible option for industry, especially since high COD removal can potentially be achieved if UF is operated in series. The process was characterised by high initial fluxes followed by rapid fouling due to cake formation, which dominated, and pore blockage. The excess cake formation induced cake filtration.

The high feed organic load and particle size distribution caused inevitable fouling, controlling the degree with which each fouling mechanism occurred, and limited the highest achievable process performance. However, TMP dictated the severity of fouling and its resulting effect on the flux and organic removal, within the range specified as a result of the feed characteristics. This study demonstrates the potential for UF as a pre-treatment method for process water in a recycled paper mill using 100% RCF, a critical step in implementing the kidney strategy and achieving water system closure for these challenging processes.

CRediT authorship contribution statement

Hans Cainglet: conceptualisation, methodology, validation, formal

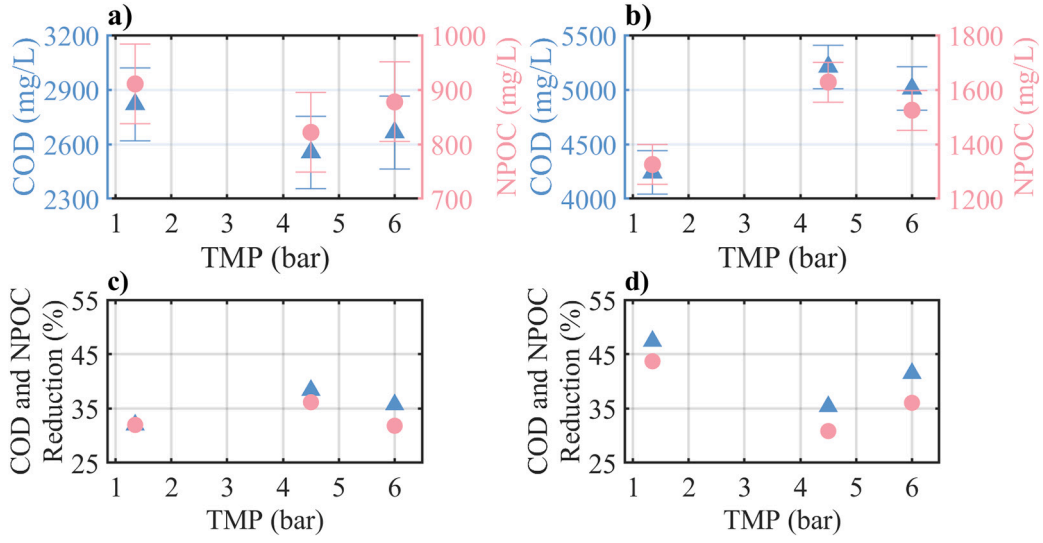

Fig. 10. COD (blue coloured triangles) and NPOC (salmon coloured circles) loads and percent reduction for 100% and 50% PW permeates at different TMP; a) 50% PW permeate organic load; b) 100% PW permeate organic load; c) 50% PW organic load reduction (%); d) 100% PW organic load reduction (%).

analysis, investigation, writing-original draft, visualisation; **Tomas Saavedra**: conceptualisation, methodology, software, formal analysis, investigation, writing- original draft; **Stefan Bürgmayr**: conceptualisation, writing- review & editing, project administration; **Jianhua Zhang**: methodology, investigation, writing- review & editing; **Zongli Xie**: methodology, investigation, writing- review & editing; **Gil Garnier**: conceptualisation, project administration, writing- review & editing, funding acquisition; **Joanne Tanner**: conceptualisation, writing- review & editing, supervision, funding acquisition.

Declaration of competing interest

The authors declare that they have no known competing financial interests or personal relationships that could have appeared to influence the work reported in this paper.

Acknowledgements

The authors would like to acknowledge Dr Parama Banerjee, Dr Hasina Yeasmin, and Prof. Udo Bach for their supervision and feedback, Derrick Ng (CSIRO) for COD analysis, and Visy Industries for the process water samples, support, and technical assistance. Project support was provided by the Australian Research Council ITRH Processing Advanced Lignocellulosics (IH170100020). Tomas Saavedra was supported by the National Agency for Research and Development (ANID) through the Scholarship Program MAGISTER BECAS CHILE/2018 – 73190555.

Appendix A. Supplementary data

Supplementary data to this article can be found online at https://doi.org/10.1016/j.jwpe.2021.102407.

References

[1] M. Eugenio, D. Ibarra, R. Sampedro, E. Espinosa, Alternative raw materials for pulp and paper production in the concept of a lignocellulosic biorefinery, Cellulose 16 (11) (2019) 1–26.
[2] E. Negaresh, Reclamation of Newsprint Mill Effluent Using Membrane Technology, 2012.
[3] M. Salo, Environmental Best Practices in the Forest Cluster IR-00-015, International Institute for Applied Systems Analysis, Laxenburg, 1999.
[4] R. Miranda, A. Blanco, C. Negro, Accumulation of dissolved and colloidal material in papremaking- application to simulation, Chem. Eng. J. 148 (2–3) (2009) 385–393.
[5] M. Mänttäri, M. Nyström, Utilization of membrane processes in treating various effluents generated in pulp and paper industry, in: K. Anil, S.H. Syed, A. Sastre (Eds.), Handbook of Membrane Separations: Chemical, Pharmaceutical, Food, and Biotechnological Applications, CRC Press, Boca Raton, 2009, pp. 981–1006.
[6] S. Xia, J. Nan, R. Liu, G. Li, Study of drinking water treatment by ultrafiltration of surface water and its application to China, Desalination 170 (1) (2004) 41–47.
[7] Y. Zhang, C. Ma, F. Ye, Y. Kong, H. Li, The treatment of wastewater of a paper mill with integrated membrane process, Desalination 236 (2009) 349–356.
[8] D. Richardson, L. Bloom, R. Elizabeth, Selective removal of inorganic salts from effluent by multistage membrane treatment, Appita (2007) 239–243.
[9] B. Allender, G. Covey, D. Shore, Low-effluent recycled paper mills, in: Appita Annual Conference, 2010.
[10] E. Moslehi, Integrating Membrane Filtration for Water Reuse in Tissue Mill, KTH Royal Institute of Technology, Stockholm, 2018.
[11] D. Richardson, L. Blom, E. Reeves, Pilot Plant Investigations Into the Feasibility of Membrane Treatment of Paper Machine and Deinking Plat Filtrates, 2008, pp. 383–387.
[12] J. Crittenden, R. Trussell, D. Hand, K. Howe, G. Tchobanoglous, Membrane filtration, in: MWH's Water Treatment: Principles and Design, Third edition, John Wiley & Sons, Inc, Hoboken, 2012, pp. 819–902.
[13] J. Hermia, Constant pressure blocking filtration laws—application to power law non-Newtonian fluids, Trans. IChemE 60 (1982) 183–187.
[14] M. Sousa, J. Lora-Garcia, M.-F. López-Pérez, Modelling approach to an ultrafiltration process for the removal of dissolved and colloidal substances from treated wastewater for reuse in recycled paper manufacturing, J. Water Process Eng. 21 (2018) 96–106.
[15] Y. Xu, Y. Li, Y. Hou, Reducing ultrafiltration membrane fouling during recycled paper mill wastewater treatment using pretreatment technologies: a comparison between coagulation and Fenton, Chem. Technol. Biotechnol. 94 (3) (2018).
[16] R. Baker, Membrane Technology and Applications, Third Edition, California: Wiley, 2012.
[17] R.B. Baird, A.D. Eaton, E.W. Rice, A.P.H. Association, A.W.W. Association, W. E. Federation, Standard Methods for the Examination of Water and Wastewater, 23d ed., American Public Health Association, American Water Works Association, Water Environment Federation, Washington D.C., 2017.
[18] ASTM D5090-90, "Standard Practice for Standardizing Ultrafiltration Permeate Flow Performance Data", ASTM International, West Conshohocken, 2001.
[19] S. de Barros, C. Andrade, E. Mendes, L. Peres, Study of fouling mechanism in pineapple juice clarification by ultrafiltration, J. Membr. Sci. 215 (2003) 213–224.
[20] L. Song, Flux decline in crossflow microfiltration and ultrafiltration: mechanisms and modeling of membrane fouling, J. Membr. Sci. 139 (1998) 183–200.
[21] V.V. Tarabara, R.M. Hovinga, M.R. Wiesner, Constant transmembrane pressure vs. constant permeate flux: effect of particle size on crossflow membrane filtration, Environ. Eng. Sci. 19 (2) (2002) 343–355.